Hindawi
Advances in Civil Engineering
Volume 2020, Article ID 8885849, 20 pages
https://doi.org/10.1155/2020/8885849

Research Article

Study on the Rheological Failure Mechanism of Weakly Cemented Soft Rock Roadway during the Mining of Close-Distance Coal Seams: A Case Study

Wenkai Ru,[1] Shanchao Hu ,[1,2] Jianguo Ning,[1] Jun Wang,[1] Qingheng Gu,[1] Yong Guo,[1] and Jing Zuo[1]

[1]*State Key Laboratory of Mining Disaster Prevention and Control Co-Founded by Shandong Province and the Ministry of Science and Technology, Shandong University of Science and Technology, 579 Qianwangang Road, Qingdao, China*
[2]*State Key Laboratory of Coal Resources and Safe Mining, China University of Mining and Technology, No. 1 University Road, Xuzhou, China*

Correspondence should be addressed to Shanchao Hu; mining2@126.com

Received 9 May 2020; Revised 15 July 2020; Accepted 20 July 2020; Published 31 July 2020

Academic Editor: Bisheng Wu

During the mining of the shallow-buried and close-distance multiple coal seam, the rheological failure of the surrounding weakly cemented soft rock of the roadway in the lower coal seam under the concentrated stress is very rare. However, the stress on the roof of the upper coal seam is transmitted down through the residual pillar, resulting in this situation. Taking the Gaojialiang coal mine which is located in the mining areas of western China as the research object, the failure mechanism of the roadway roof under the residual coal pillar in the shallow-buried and close-distance multiple seam is studied in combination with field monitoring and numerical simulation. Furthermore, suggestions on the roadway support under such geological conditions are proposed. The results show that the residual coal pillar in the working face of the lower coal seam gradually collapses during the mining of the shallow-buried and close-distance multiple coal seam. The concentrated stress transferred by the coal pillar increases further, which makes the roof stress of the lower coal seam roadway to increase continuously. In addition, the stress of the roadway roof also increases further due to the rotation of the broken rock above the goaf, and the peek region of stress moves to the nongoaf area. Combining the heavy concentrated stress and weakly cemented property, the shallow-buried surrounding rock shows rheological behavior and failure. Therefore, we must pay more attention on the creep failure of the roadway roof under the action of the residual coal pillar even in the shallow-buried coal seam.

1. Introduction

Shallow-buried Jurassic coalfields abound in western China widely, which boasts the abundant reserves. They are featured by rich minable coal seams and close interlayer spacing [1, 2]. When mining the close-distance coal seams, the working faces of the upper and lower coal seams are usually arranged in parallel [3]. However, due to the geological conditions such as faults and coal-free areas, staggered arrangement appears inevitably [4–6]. When the stopping roadway of the lower coal seam is arranged under the section coal pillar left by the upper coal seam, coal pillar loading can be calculated based on the assumption that the coal pillar bears the loading of the overlying stratum [7, 8] within its influenced area according to the tributary area theory, and the concentrated stress causes the failure of the roadway [9–12].

In order to figure out the failure mechanism of the surrounding rock in the goaf, the residual coal pillar, or the solid coal, some scholars have done a lot of research on the law of mine pressure when mining the shallow-buried and close-distance coal seam by means of the field test, theoretical analysis, and numerical simulation. First of all, the physical and mechanical properties and components of the

shallow-buried weakly cemented rock have been studied. It was found that the lithology of weakly cemented rock is mainly composed of sandy mudstone and fine sandstone [13, 14]. And, mudstone contains a high proportion of clay minerals, which easily leads to disintegration and high inflation under certain stress [15]. Based on this, some scholars have used the conventional compression test [16], shear test [17], and acoustic emission test [18] and found that the failure evolution and stress distribution of the weakly cemented surrounding rock had had obvious time effects [19–21]. Furthermore, the rock crept steadily under the lighter stress [22].

Subsequently, the concentrated loading formed by the residual coal pillar in the upper coal seam will be transferred downward through the floor strata, forming a stress-concentrated area in the floor. Consequently, the concentrated stress transferring rule of the residual coal pillar should be determined [23, 24]. Using the tributary area theory, the stability analysis method of coal pillars [25] and the Wilson and Carr method [26] are developed. By establishing the stress increment model of the pressure-relief mining floor [27, 28], it can be obtained that the floor of the coal seam after pressure-relief mining can be divided into four areas in the aspects of floor rupture area (arc), stress-relaxed area (parabola), stress-concentrated area (oval), and original rock stress area. Only when the lower coal roadway is arranged in the stress-relaxed area of the coal pillar floor can the stability of the roadway be more easily guaranteed.

In the end, it is necessary to analyze the stability of the floor roadway during the mining of the close-distance coal seam. The reason is that the floor of the coal pillar is the roadway roof of the lower coal seam. Based on the elasto-plastic mechanics and fracture mechanics under unloading conditions, the dynamic distribution and evolution laws of fractures in different stress areas in the floor under the influence of mining can be achieved [29–31]. At the same time, the deformation caused by the mining of the upper coal seam to the floor is determined [32]. The failure characteristics and depth of the interval rock under different mining conditions are generally determined by theoretical analysis, field monitoring, and numerical simulation. And, numerical simulation because of its simplicity has been commonly used in longwall mining to investigate mining-induced rock mass responses [33].

It can be found that remarkable achievements have been made in the studies of strength properties of weakly cemented rock and the stress transmission of the residual coal pillar. However, due to the shallow burial of coal seams in western China, the rheological phenomenon of weakly cemented rocks under concentrated stress has not attracted people's attention. As a result, problems of rheological failure of the roadway under the long-term action of concentrated loading of coal pillars have appeared [34], which has brought safety risks during production. This paper takes the shallow-buried and close-distance coal seam in western China as the research object. In combination with the field monitoring and numerical simulation, it studies the failure mechanism of the roadway roof under the residual coal pillar in the shallow-buried and close-distance multiple seam and provides the basis for the roadway support under similar geological conditions [35, 36].

2. Mechanical Properties of Weakly Consolidated Soft Rock

There are 6 coal layers that can be mined in the Gaojialiang coal mine in western China. Currently, 2-2 upper and 2-2 middle coal seams are mainly mined. The depth and average thickness of the 2-2 upper coal seam are 165 m and 1.71 m, respectively, while those of the 2-2 middle coal seam are 170 m and 2.73 m, respectively. The distance between the two coal seams is 6.65~11.9 m, which is counted as a close-distance coal seam. The weakly cemented rock, between the two coal seams, is composed of sandy mudstone and siltstone. It belongs to the typical weakly consolidated soft rock strata.

For the purpose of figuring out the mechanical mechanism of deformation and failure of the surrounding rock of the roadway under the residual coal pillar and providing the basis for the design of the roadway support under similar conditions, the component analysis and the creep test of the stratum between layers of Gaojialiang are carried out.

2.1. Analysis on Components of Strata. The components and parameters of physical mechanics of the interval strata are measured, and the components of strata are shown in Table 1. The interval strata is mainly composed of sandy mudstone, and the sandy mudstone is mainly composed of kaolinite and illite. Both are common clay minerals with a low hardness. The tensile and compressive strengths of sandy mudstone are 11.5 MPa and 3.5 MPa, respectively, and its elastic modulus is 13.7 GPa. It can be seen that its strength is generally low, so the surrounding rock of the roadway belongs to the typical weakly cemented soft rock.

2.2. Creep Test on Weakly Cemented Rock. As mentioned above, some scholars have carried out rheological tests on the shallow-buried weakly cemented rock and found that it would exhibit rheological behavior under lower stress [37–39]. Therefore, the sandy mudstone obtained in the Gaojialiang mine is selected for the creep test. A core is taken to prepare a standard sample of ϕ 50 mm × 100 mm, and graded-loading creep tests are performed. The failure strength of the specimens under 1.5 MPa confining creep compression is 14.5 MPa. The time-history curve and the creep properties curve under 1.5 MPa confining pressure are shown in Figure 1.

According to the curve of creep loading and considering the axial, lateral, and volume deformation characteristics of the rock, the stress-strain isochronous curve cluster under 1.5 MPa confining pressure is drawn, as shown in Figures 2(a)–2(c). For the three-way creep isochronous curve cluster, there are two inflection points among which point A is the sign of creep deformation and B is the strongly nonlinear plasticity after deformation. The stress at point A can be regarded as the threshold value of damage generation and B as the long-term strength index σ_∞ of the rock sample.

Table 1: The components of the shallow-buried strata.

Lithology	Kaolinite	Illite	Chlorite	Iraq/middle layer
Coarse sandstone	29	15	5	—
Mudstone	29	15	5	—
Fine sandstone	25.4	16.37	38.82	<10
Medium sandstone	25.4	36.93	31.12	<10
Sandy mudstone	—	55	25	—

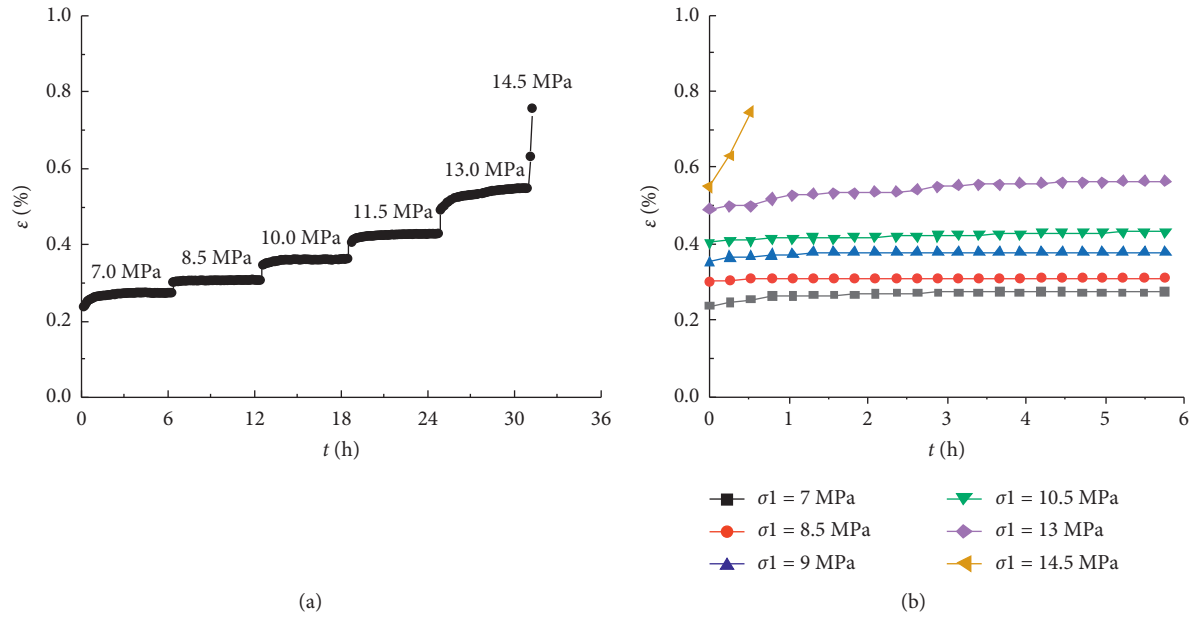

Figure 1: Under 1.5 MPa confining pressure, (a) time-history curve of strain and (b) creep characteristic curve.

The long-term strength of the specimen under 1.5 MPa confining pressure is 11.7 MPa. The long-term strength is slightly less than the rheological strength.

3. Geological Overview and Roadway Damage

In order to further verify the rheological failure characteristics and mechanism of weakly consolidated surrounding rock under a concentrated load, we conducted field monitoring in the Gaojialiang coal mine.

3.1. Geological Overview. At present, the 2-2 upper coal seam has been completed, while the 2-2 coal seam is being mined in the Gaojialiang coal mine. Affected by the coal-free area, most of the roadways in the 2-2 middle coal seam mined at this stage are arranged in the goaf of the 2-2 upper coal seam or the residual coal pillar. Figure 3 presents the layouts of the roadways and goafs. The 20314 auxiliary haulage roadway is located in the 2-2 middle coal seam, which is arranged in cross with multiple goafs on the overlying coal seam. And, the roadway is located under the upper coal seam goaf or the residual coal pillar. As a result, the roof of the 20314 auxiliary haulage roadway is complexly stressed. In particular, when it is under the residual coal pillar, problems such as the sink of the roadway roof, the bulge of the floor, the rib spalling, and the break of the bolt and the anchor cable often occur.

3.2. Field Monitoring Method. In order to observe the surface and deep displacements of the surrounding rock of the roadway under the residual coal pillar in the upper coal seam, the mechanism of deformation and failure can be revealed and the basis for the surrounding rock support measures can be provided. A station is arranged in the 20314 auxiliary haulage roadway to determine the variation laws of the roadway displacement and the stress of the supporting body. Based on the intersection characteristics of the working faces of the 2-2 upper and 2-2 middle coal seams, the monitoring plan towards the lower coal seam roadway is formulated. 1# is arranged under the junction of the coal pillar and goaf, 2#, 3#, and 5# are placed under the coal pillar, and 4# is arranged under the solid coal. Two measuring points with a 5 m spacing are set in each station. Each station mainly includes the following equipment for testing: anchor (cable) dynamometer, borehole stress meter, borehole drilling TV, etc. Figure 4 depicts the arrangement of the monitoring instrument.

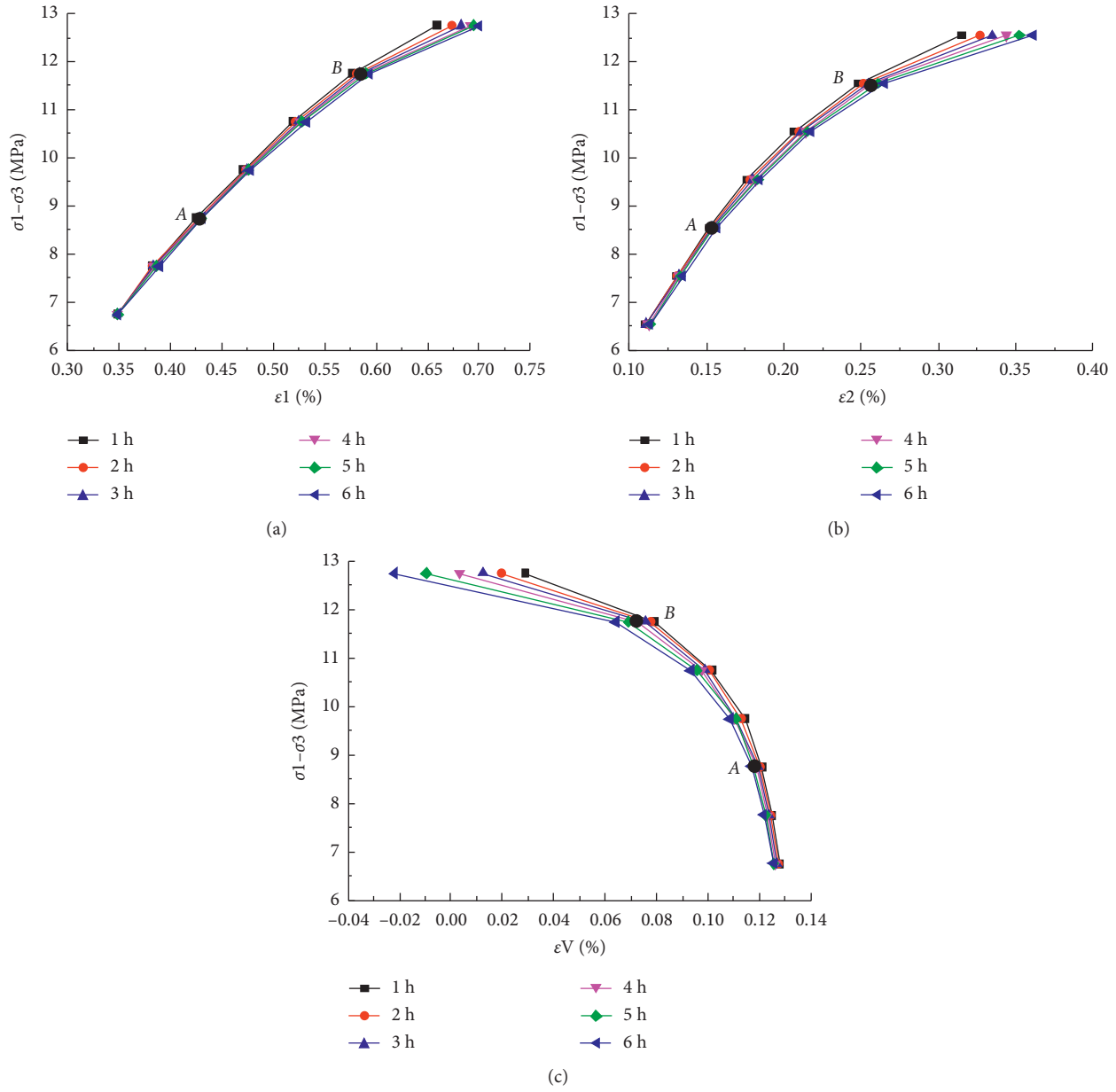

Figure 2: Stress-strain isochronous curve cluster: (a) axial strain; (b) lateral strain; (c) volume strain.

3.3. Deformation and Failure of Roadway

3.3.1. Macroscopic Failure of the Surrounding Rock of Roadway. When the P20314 working face is moved to 900 m, the surrounding rock of the roadway at 44 m north of the auxiliary haulage roadway from the quadruple roadway shows deformation and failure. Problems such as the sink of the roadway roof, the bulge of the floor, and the rib spalling appear. Figure 5 reveals the deformation and failure range (54 m) of the surrounding rock. When the roadway stabilizes again, the roadway roof in the range of 6~18 m on the right side sinks in an arc way, while in the range of 18~36 m on the left side shows a step-type sinking with 0.6~0.8 m height. Due to a greater sink of the roof, some bolts (cables) are broken and dropped and some of the single hydraulic props are crushed. Figure 6 shows the deformation and failure forms of the surrounding rock of the roadway.

3.3.2. Roadway Displacement Variation

(1) Roadway Surface Displacement. Surface displacement of the roadway includes the subsidence convergence of the roadway roof and the displacement convergence of the two sides. Surface displacements observed at 4# and 5# stations vary with time, as shown in Figures 7(a) and 7(b). It can be known that both subsidence and displacement convergences increase first and then stabilize as time goes by. In the first 12 days, the surface displacement changes barely. However, the surface displacement of the surrounding rock suddenly

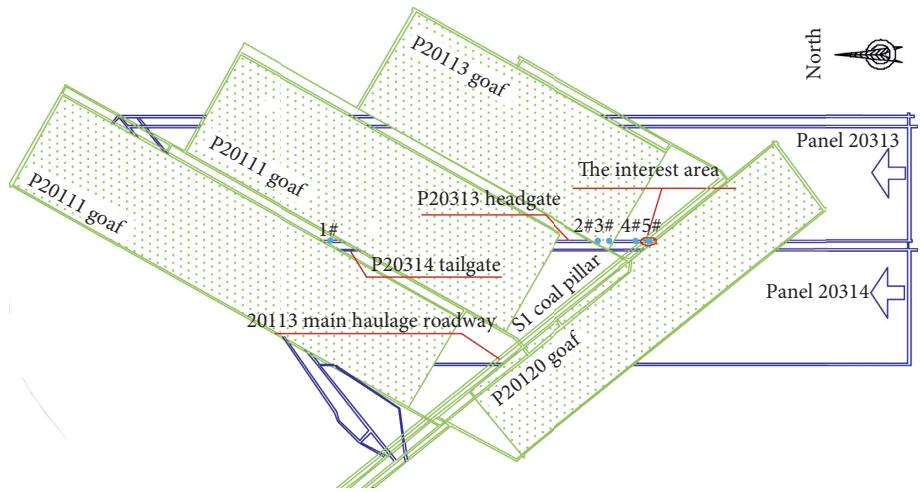

Figure 3: Layouts of the 2-2 upper and 2-2 middle coal seams.

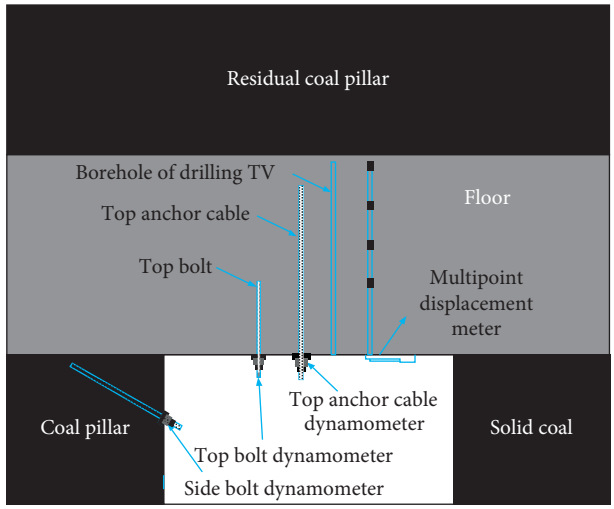

Figure 4: Arrangement of the monitoring instrument.

increases on the 13th day and stabilizes again after the 19th day. As the measuring points at the 5# station are located under the residual coal pillar, the surrounding rock of the roadway is seriously deformed because it suffers from a high concentrated stress. Furthermore, 5#-1 is the worst part of the station in which the maximum subsidence and displacement convergences reach 328 mm and 282 mm, respectively. By contrast, the subsidence convergence of the roof and the displacement convergence of the two sides at the 4# station change slightly, showing 27 mm and 91 mm, respectively. The reason is that the two measuring points at the 4# station are located under the solid coal, and the stress of the surrounding rock of the roadway is smaller than that of the lower part of the coal pillar.

(2) Displacement of Deep Roadway. Figures 8(a) and 8(b) show the displacement curves of the deep roadway roof at 4# and 5# stations. Similar to the variation law of the surface displacement of the roadway, the displacement of each measuring point in the deep also stabilizes first and then increases and stabilizes finally. For the shallow base point—depth measuring point with 2.5 m—two measuring points at the 4# station are located under the solid coal where point 4#-1 is far from the boundary of the solid coal and the displacement of the deep roof is 14 mm. Point 4#-2 is arranged at the boundary, which is greatly suffered from the concentrated stress than 4#-1. Consequently, the displacement of the deep roof is 16 mm. And, the two measuring points at the 5# station are arranged under the residual coal pillar, which are also greatly suffered from the concentrated stress, and the displacements are 16 mm and 13 mm, respectively. For the deep base point—depth measuring point with 4.5 m—the displacements of the deep roof of the two measuring points at the 4# station change slightly, while the displacement of the point 5#-1 is 18 mm at point 5#-2 is 12 mm.

3.3.3. Stress Variation of Roadway Support. Figures 9(a)–9(c) present the stress variations of bolts (cables) at 4# and 5# stations. As time moves, the stresses of the bolts (cables) in the roof and on the sides increase first and then stabilize. The 5#-1 measuring point is located under the residual coal pillar, with the completion of mining in the 20314 working face; the stress here is the most concentrated, and the force of the supporting body changes the most. Specifically, the forces of the anchor cable and the bolt in the roof increase by 40 kN and 32 kN, respectively, and the force of the bolt on the two sides increases by 18 kN. Correspondingly, the 4#-1 measuring point is arranged under the solid coal, which is less affected by the stopping of the P20314 working face. Therefore, the force at this point changes slightly, and forces of the anchor cable and the bolt in the roof increase by 20 kN and 12 kN, respectively. And, on the two sides, the fore of the bolt increases by 7 kN.

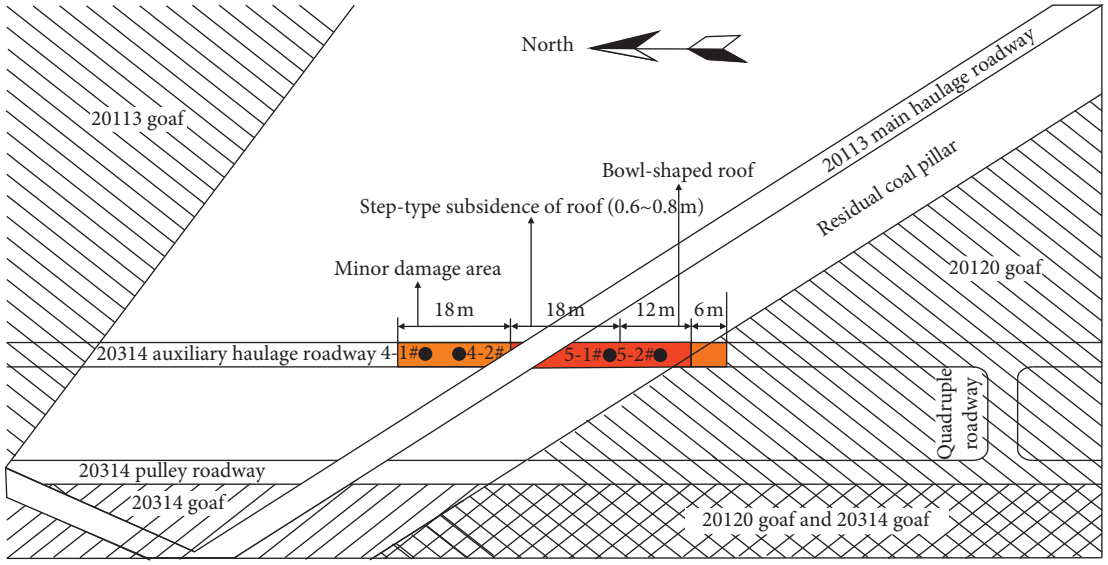

Figure 5: Deformation and failure range of the roadway.

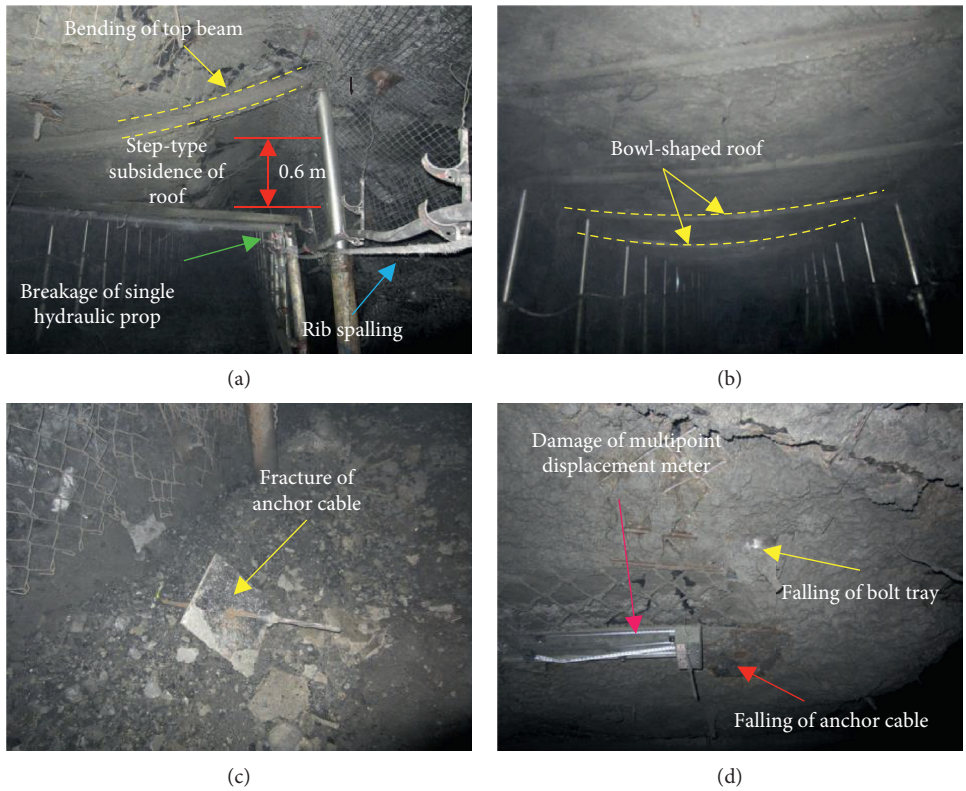

Figure 6: Deformation and failure forms of the surrounding rock of the roadway.

3.3.4. Drilling TV Monitoring Results. The monitoring results of some boreholes are shown in Figure 10. According to the peep results of the borehole, it can be obtained that there are many fracture areas within 0–2.72 m at the point 4#-2 and within 0–2.60 m at the point 5#-1. The roof rock in both these areas is seriously deformed and express rock fractures. The phenomenon of separation appears rarely. When peeping the drilling (depth) in the range of 2.72 m~3.29 m at the point 4#-2 and of 2.60 m~3.33 m at the point 5#-1, the roof rock is slightly deformed and holds overall integrity. Furthermore, when peeping the drilling (depth) over 4.7 m, the surrounding rock roof is basically intact and there is no small separation layer. It should be noted that it fails to observe the failure of the surrounding rock roof caused by

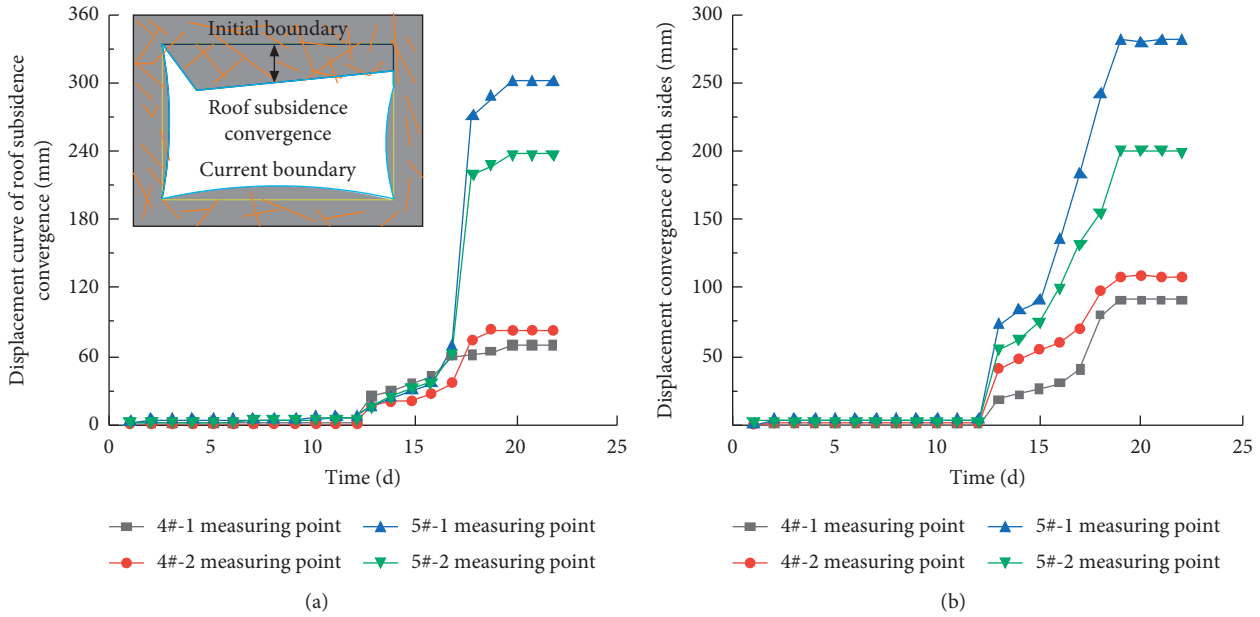

Figure 7: Displacement curve of the roadway surface: (a) displacement curve of roof subsidence convergence; (b) displacement convergence of both sides.

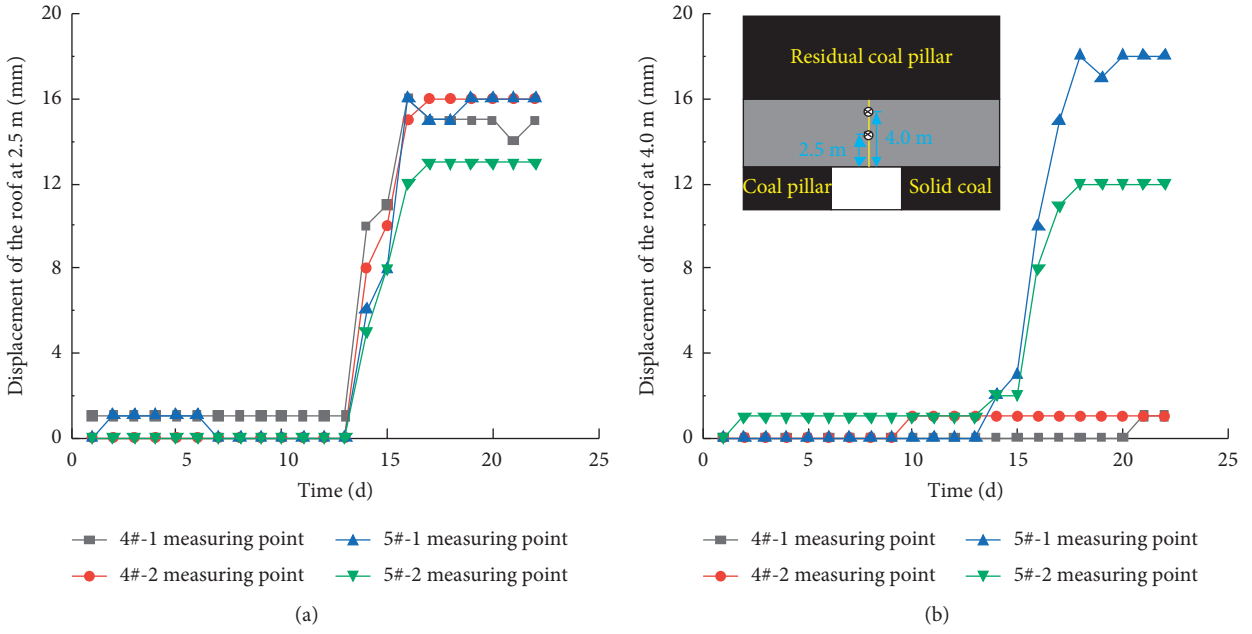

Figure 8: Displacement curve of the deep roof: (a) displacement of the roof at 2.5 m; (b) displacement of the roof at 4.0 m.

step-type subsidence at one side of the roadway because the TV drilling is arranged in the middle of the roadway in the earlier stage.

4. Numerical Simulation of Rheological Damage in Close-Distance Coal Seam Roadway

4.1. Numerical Model. In order to further study the deformation and failure law of the 2-2 middle coal seam roadway with the stopping of working face, the numerical calculation model is established by using the ANSYS software. The model size is 400 m × 300 m × 119 m, as shown in Figure 11. Grid elements of the 20314 auxiliary haulage roadway (the main area which is observed for deformation and failure study of the surrounding rock of the roadway) are densified, and the minimum length is 0.5 m. In addition, the horizontal and vertical directions of the model are limited. A vertical load of 5.0 MPa is applied over the model to replace the unmodeled rock formation above.

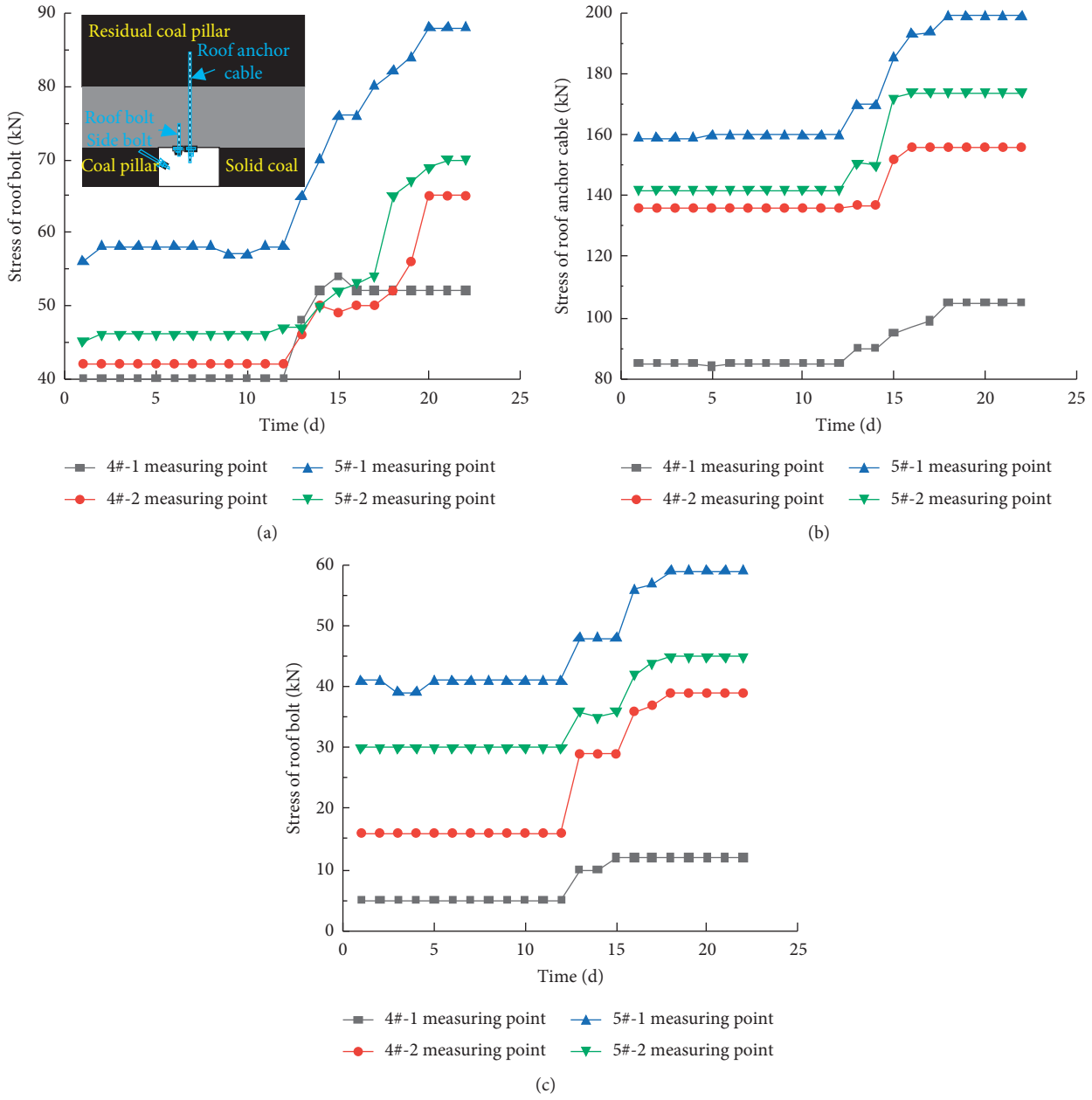

Figure 9: Stress curve of the anchorage body: (a) stress of the roof bolt; (b) stress of the roof anchor cable; (c) stress of the side bolt.

FLAC3D software is used in the numerical simulation, and the Mohr–Coulomb constitutive model is overall used in the calculation model. For studying the deformation and failure characteristics of the surrounding rock of the roadway in the lower coal seam under a concentrated load, the CVISC rheological constitutive model is adopted in the surrounding rock of the roadway in the active area of residual coal pillar [40]. Table 2 depicts the parameters of numerical calculation. During the numerical simulation, the roadway and the working face of the 2-2 upper coal seam are first excavated to form a goaf and a section coal pillar, and these 2-2 middle coal seams are excavated in sequence.

4.2. Numerical Simulation Results. During the mining of the 2-2 upper coal seam, a residual coal pillar with a width of 23 is formed between the 20120 goaf and the 20113 main haulage roadway. The vertical stress of the roof of the auxiliary haulage roadway under the residual coal pillar is greater than 12 MPa (Figure 12(a)). Since the 2-2 middle coal seam has not been excavated at this time, the displacement of the rock under the residual coal pillar changes slightly, ranging from 0.05 m to 0.15 m (Figure 13(a)).

As shown in Figure 12(b), during the mining of the 2-2 middle coal seam, the stresses of the residual coal pillar and the lower rock are released due to the excavation of the 20314

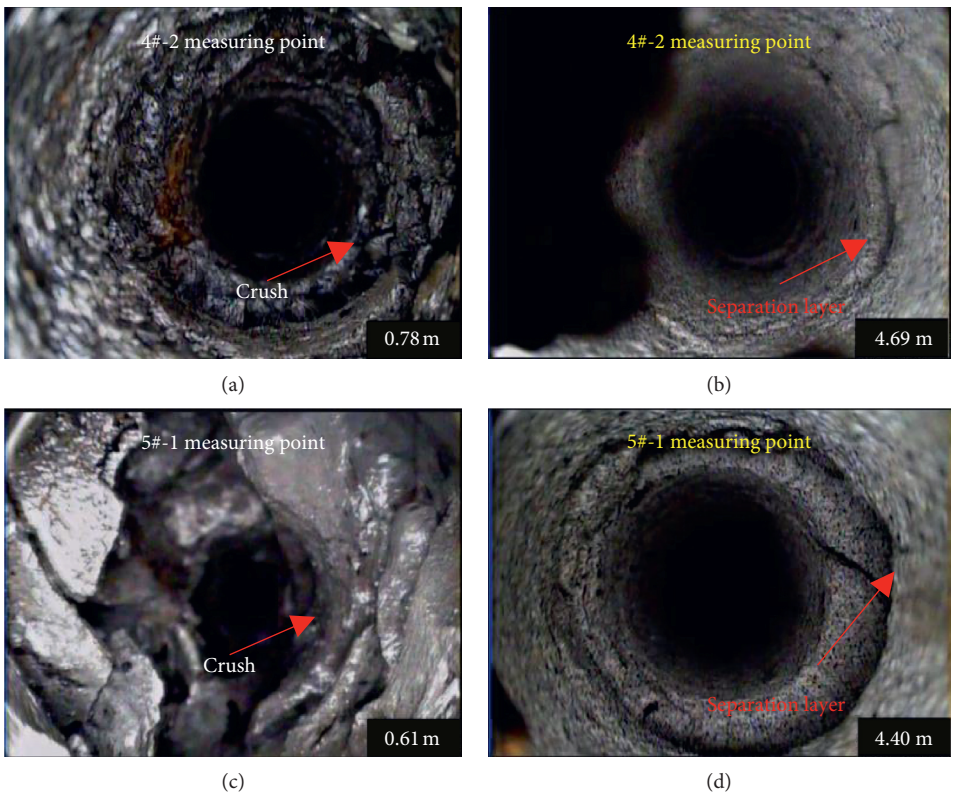

Figure 10: Images of different depths of borehole TV at two measuring points.

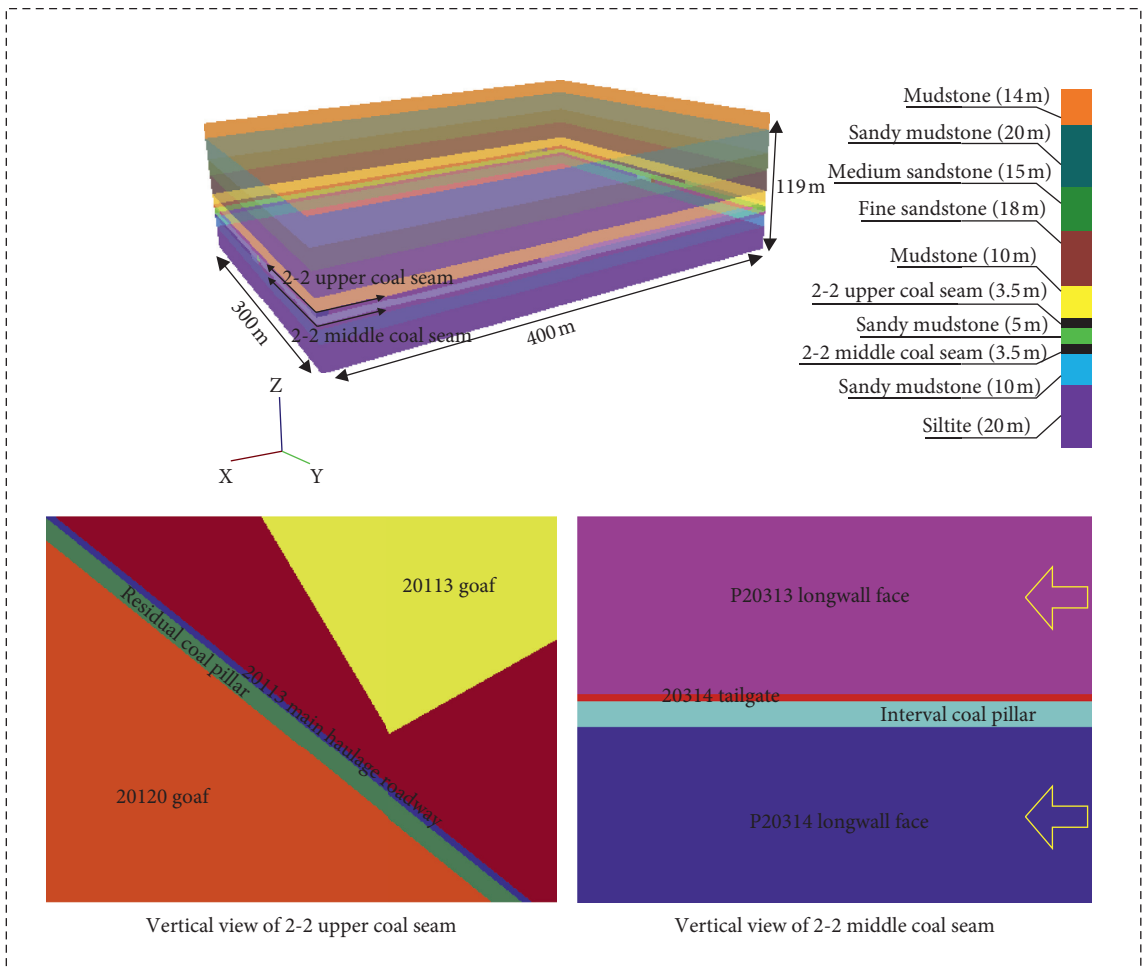

Figure 11: Numerical model.

Table 2: Mechanical properties of the coal measures that are used in the model.

Coal measures	Thickness (m)	Density ($g.cm^{-3}$)	Young's modulus (GPa)	Shear modulus (GPa)	Tensile strength (MPa)	Cohesion (MPa)	Friction angle (°)
Mudstone	14	2.30	6.2	3.5	1.1	2.3	27
Sandy mudstone	20.8	2.52	15.4	7.3	1.2	2.2	30
Medium sandstone	15.1	2.59	16.8	8.6	1.7	5.5	29
Fine sandstone	18.2	2.49	26.8	12.1	1.2	4.5	32
Mudstone	9.8	2.3	6.2	3.5	1.1	2.3	27
2-2 上 coal	3.5	1.42	1.7	1.1	1.0	2.3 (0.8)	35 (25)
Sandy mudstone	5	2.52	15.4	7.3	1.2	2.2 (0.62)	30 (22)
2-2 中 coal	3.5	1.42	1.7	1.1	1.0	2.3 (0.8)	35 (25)
Sandy mudstone	9.5	2.52	15.4	7.3	1.2	2.2 (0.62)	30 (22)
Siltstone	17.8	2.54	17.6	8.0	1.7	5.5	32

*Numbers in parentheses are residual values.

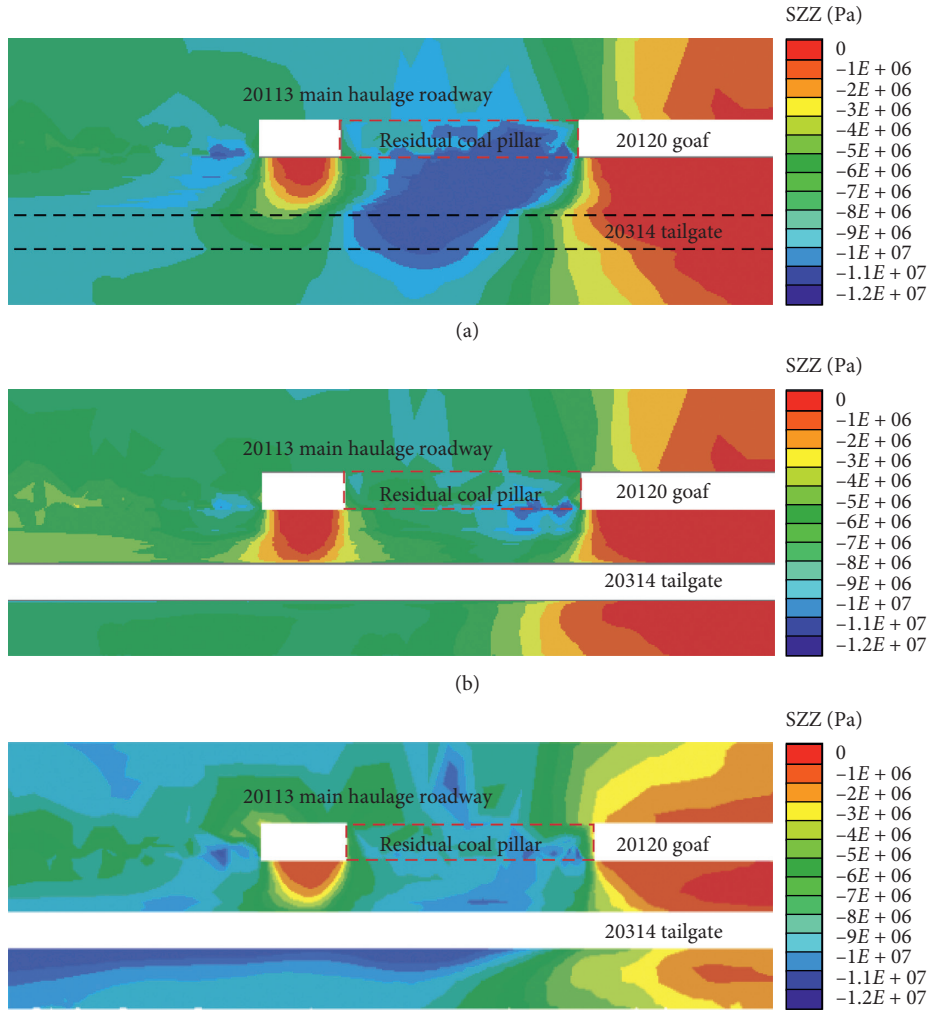

Figure 12: Stress variation of the 20314 auxiliary haulage roadway (parallel to the axis section of the roadway): (a) 2-2 upper coal seam excavation; (b) 20314 tailgate excavation; (c) 20314 panel excavation.

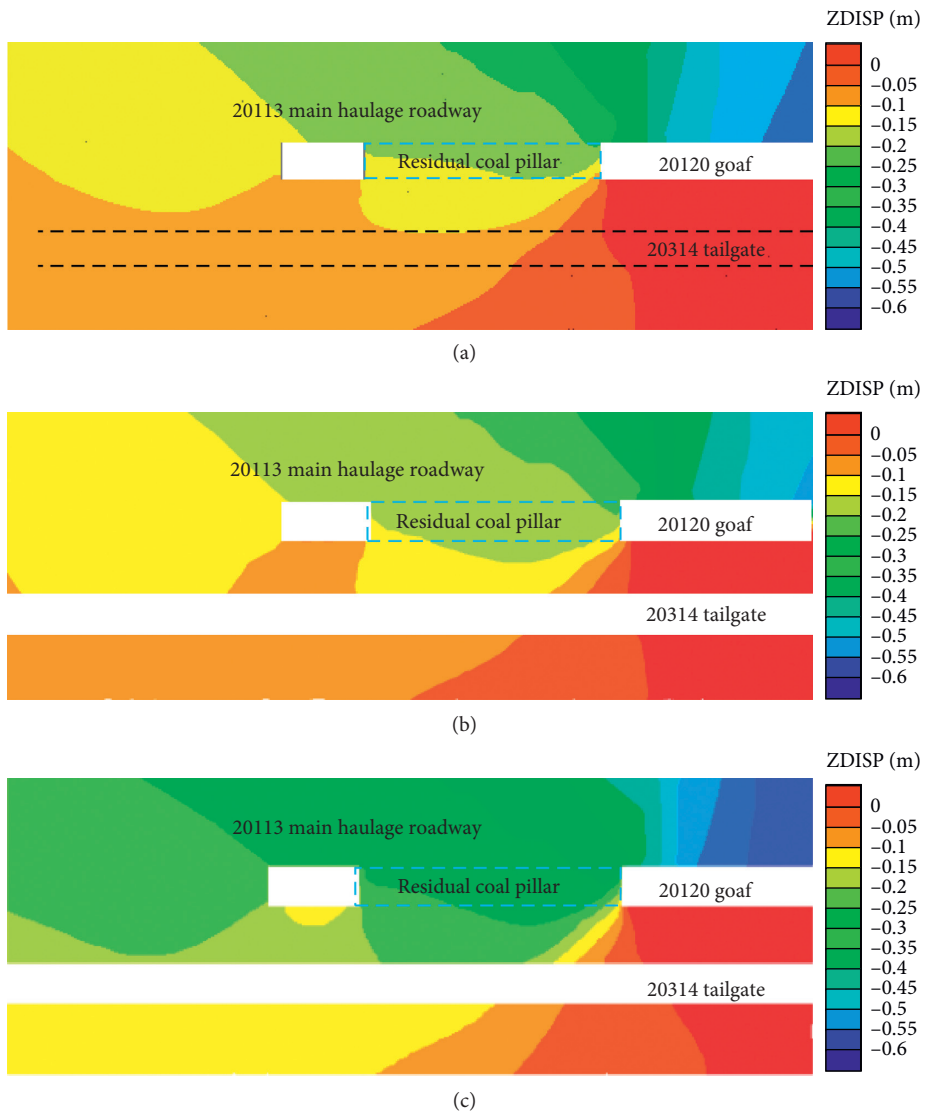

Figure 13: Displacement variation of the roof of the 20314 auxiliary haulage roadway (parallel to the axis section of the roadway): (a) 2-2 upper coal seam excavation; (b) 20314 tailgate excavation; (c) 20314 panel excavation.

auxiliary haulage roadway. Meanwhile, the vertical stress in the rock reduces significantly and is 5~9 MPa. There is no obvious displacement change of the surrounding rock of the roadway. And, the P20314 working face is further excavated. At this time, the stress concentration of the roof of the auxiliary haulage roadway appears again, and the vertical stress reaches 9~11 MPa (Figure 12(c)). Furthermore, the displacement of the roof of the 20314 auxiliary haulage roadway increases significantly (Figure 13(c)), which reaches 0.15~0.3 m.

In addition, the evolution law of the plastic area of the interval rock under the residual coal pillar during the mining of two coal seams is analyzed. It can be seen that after the excavation of the 2-2 upper coal seam, the plastic area appears in the floor (roof of the 20314 auxiliary haulage roadway) of the residual coal pillar (Figure 14(a)), but the deformation range is small. After the excavation of the 20314 auxiliary haulage roadway, the plastic area of the rock under the residual coal pillar slightly expands (Figure 14(b)). When the P20314 working face moves to the active area of the residual coal pillar, the goafs in the 2-2 upper coal seam and the middle coal seams connect together. The broken roof develops upwards, and the increasing roof load is further transferred downward through the residual coal pillar. As a result, the plastic area of the surrounding rock of the roadway in the 2-2 middle coal seam increases sharply, and the entire thickness of the interval rock in some areas is deformed (Figure 14(c)).

Based on the above analysis, the vertical stress variation of the roof of the 20314 auxiliary haulage roadway goes through three stages. In the first stage, the remaining coal pillars are formed owing to the excavation of each roadway and working face in the 2-2 upper coal seam, which causes the vertical stress of the roadway roof to increase sharply, and the roof stress is concentrated. In the second stage, the vertical stress of the roof is partly released due to the

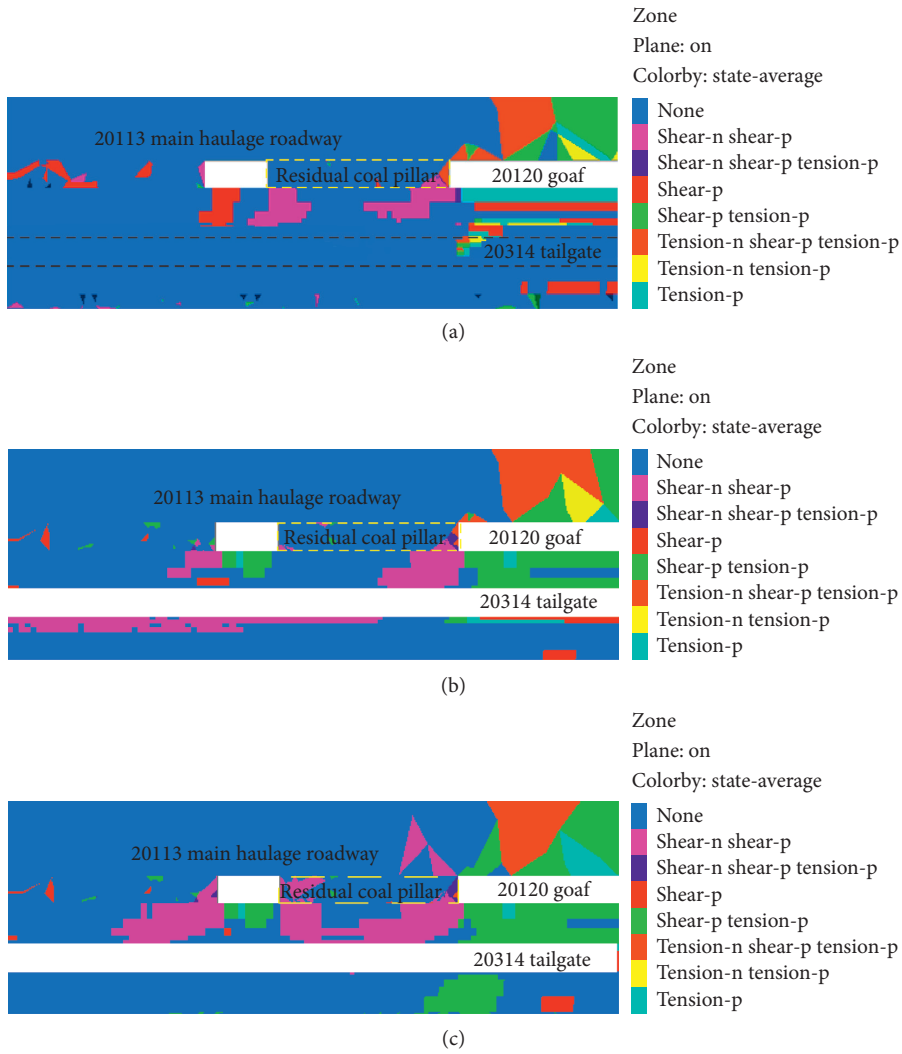

Figure 14: Section variation of the plastic area that is parallel to the 20314 auxiliary haulage roadway (parallel to the axis section of the roadway): (a) 2-2 upper coal seam excavation; (b) 20314 tailgate excavation; (c) 20314 panel excavation.

excavation of the 20314 auxiliary haulage roadway, and the vertical stress reduces and the roadway roof is not deformed. In the third stage, the stress concentration point of the coal pillar towards the 20113 centralized main haulage roadway is due to the stopping of the P20314 working face. At this time, the vertical stress of the roadway roof increases again, causing the deformation and failure of the roof and the surrounding rock of the roadway.

5. Analysis on Deformation and Failure Mechanism

Through the numerical simulation in Section 4, the stress on the roof of the 20314 tailgate after the excavation of the different coal face is repeated, and the evolution process of stress, displacement, and plastic zone in the process is obtained. In Section 5, the failure mechanism is analyzed based on the above evolution process. The strata above the coal seam resist caving and easily overhang for a considerable length, and thus a roof cantilever beam can form above the goaf edge after the working face has retreated. According to the field data and theoretical analysis, it can be seen that the stress variation of the roof of the 20314 auxiliary haulage roadway undergoes the following three stages.

5.1. Stage I. As shown in Figure 15(a), due to the cantilever beam formed by the stopping of the 2012 working face in the upper coal seam, the stress of the strata under the residual coal pillar increases rapidly and the edge of the coal pillar is obviously broken. Meanwhile, area "a" is at the junction of the elastic and plastic zone, and the stress concentration is obvious. Combined with the numerical simulation results, it can be concluded that the plastic zone of the roof of the auxiliary haulage roadway is small after the completion of the 2-2 upper coal seam (Figure 16(a)), and area "a" is the stress peak area. At this time, the stress and displacement variations of the roof strata are shown in Figures 17(a) and 18(a), respectively.

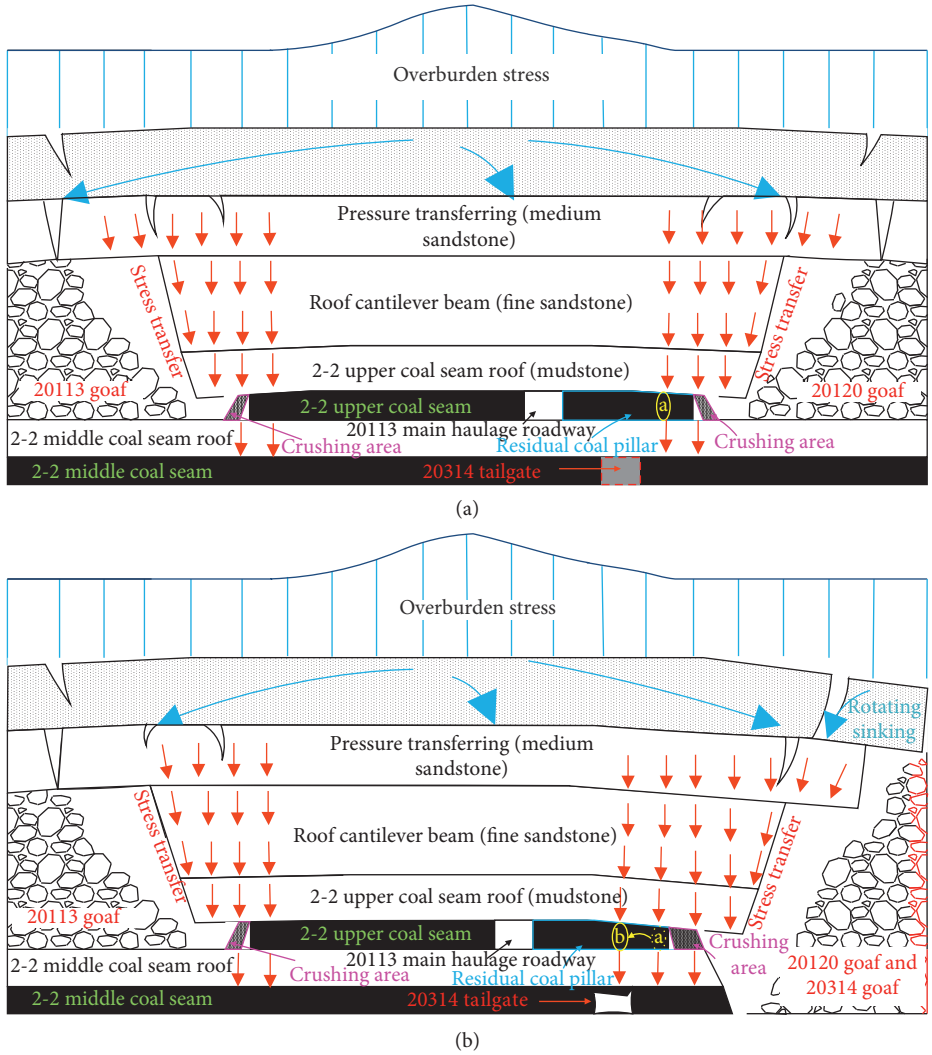

Figure 15: Stress changes under the coal pillar: (a) excavation of the 2-2 upper coal seam; (b) excavation of the P20314 working face.

5.2. Stage II. When mining the 2-2 middle coal seam, the roof movement of the 2-2 upper coal seam has stabilized. Since the size of the 20314 auxiliary haulage roadway is relatively small, the expansion range and displacement convergence of the plastic zone of the roadway roof are also small when excavating (Figures 16(b) and 18(b)) the auxiliary haulage roadway. The peak position of the stress is unchanged basically.

5.3. Stage III. As shown in Figure 15(b), a part of the P20314 working face is located under the 20120 goaf. With the stopping of the P20314 working face, the 20120 goaf continues to fall downward to connect with the goaf of the P20314 working face. Before the stopping of the 20120 working face, a part of the overlying strata of the roof has been broken. However, the strata of the roof is complete at this time, and the bearing capacity is large enough to carry the high stress under the residual coal pillar. With the stopping of the working face, the overlying fractured strata in the goaf develop further. The cantilever, due to the bending and subsidence of the fractured strata, increases the pressure on the residual coal pillar. The broken and plastic areas of the goaf increase, and the stress point of the peak moves to the center of the coal pillar. Furthermore, position "b" is just above the roof of the 20314 auxiliary haulage roadway, which is consistent with the numerical simulation results of stress concentration of the roadway roof under the residual coal pillar after the stopping of the P20314 working face (Figures 16(c) and 17(c)).

Under this structure, the movement of the basic roof fault block determines the stability of the working face roadway. The fracture span a of the fracture block is related to the length b of the working face and the periodic fracture span L:

$$a = \frac{2L}{17}\left[\sqrt{\left(10\frac{L}{b}\right) + 102} - 10\frac{L}{b}\right]. \quad (1)$$

The length of the working face b is 1611.1 m, the periodic fracture span L is 12M, and a is 14.1 m. The weight directly transferred to the coal seam is [41, 42]

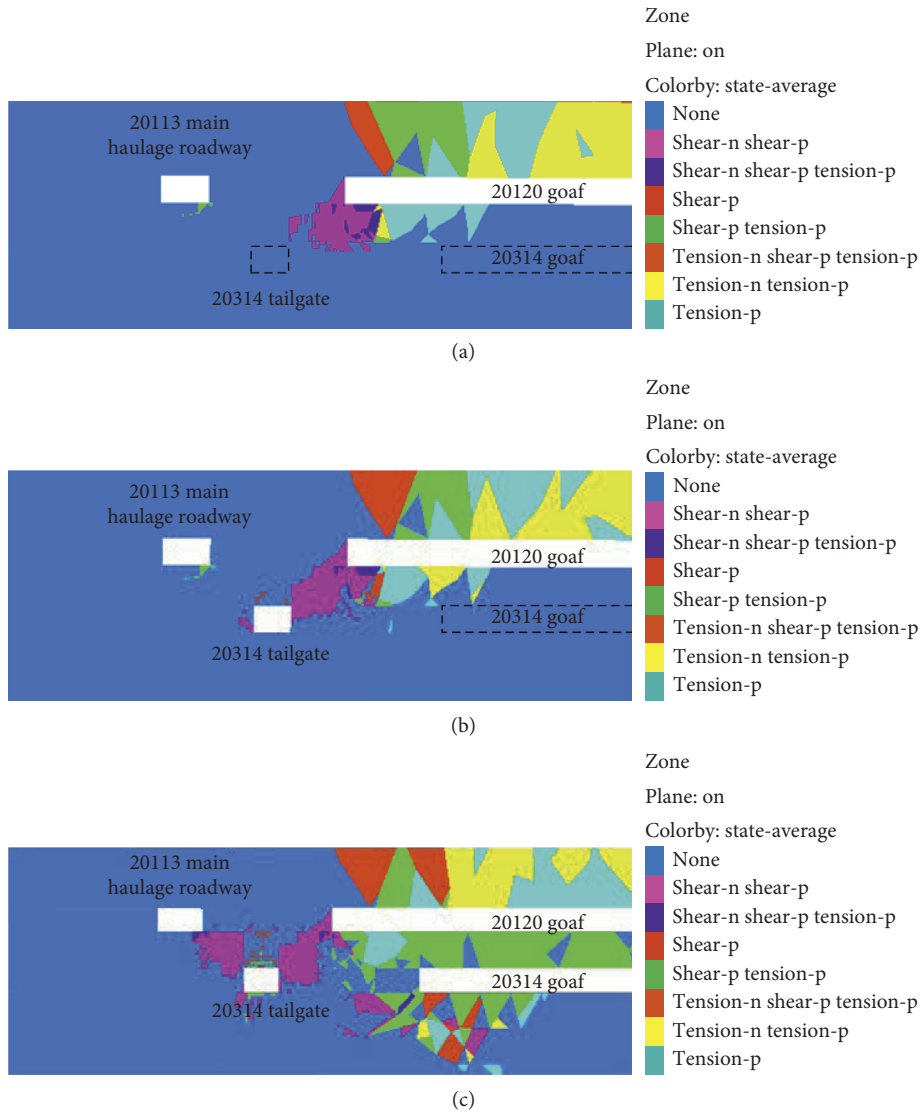

Figure 16: Nephogram of the plastic zone perpendicular to the section of the auxiliary haulage roadway (perpendicular to the axis section of the roadway): (a) 2-2 upper coal seam excavation; (b) 20314 tailgate excavation; (c) 20314 panel excavation.

$$Q = \frac{q}{2} = \frac{\gamma h a}{2}, \tag{2}$$

where γ is the average bulk density of the overlying strata, 25 kN/m^3, h is the thickness of the rock stratum, 3 m, and Q is 528.8 kN/m. The forces transmitted to the coal seam are

$$\sigma = \begin{cases} \sigma_{\max} \sin \alpha, & (0 \le x \le H), \\ 2\sigma_{\max}\left(1 - \dfrac{x \sin \alpha}{2}\right), & (H \le x \le 2H), \\ 0, & (x \ge 2H), \end{cases} \tag{3}$$

where $\sigma_{\max}$ is the maximum stress $\sigma = 15.9$ MPa of the fault block on the coal seam, $\sigma_{\max} = Q \sin \alpha \tan \alpha / H$; H is the vertical distance from the fault block to the coal seam, 43 m; α is the stress influence angle of the block, 60°. By substituting the data, we can find that $\sigma_{\max} = 18.4$ MPa. When the influence angle is 60°, x is less than H, so it can be seen that $\sigma = 15.9$ MPa, which is larger than the long-term strength of the rock layer of 11.7 MPa, so rheological failure will occur under this condition.

Base on the field monitoring, it can be known that the deformation and failure of the surrounding rock of the roadway in the 20314 auxiliary haulage roadway occurs after a long period of time. Therefore, combined with theoretical analysis and numerical simulation results, it is obtained that the stress of the roof rock strata exceeds its bearing capacity and then causes the creep, and thus brings in the deformation and failure of the surrounding rock of the roadway. Furthermore, from the numerical simulation results of Figure 19, it can be seen that the forces on the top corners of the 20314 auxiliary haulage roadway and its goaf roof are significantly greater than that on the side of the P20313 working face. And, this complies with the step-type subsidence in the side roof of the P20314 working face goaf.

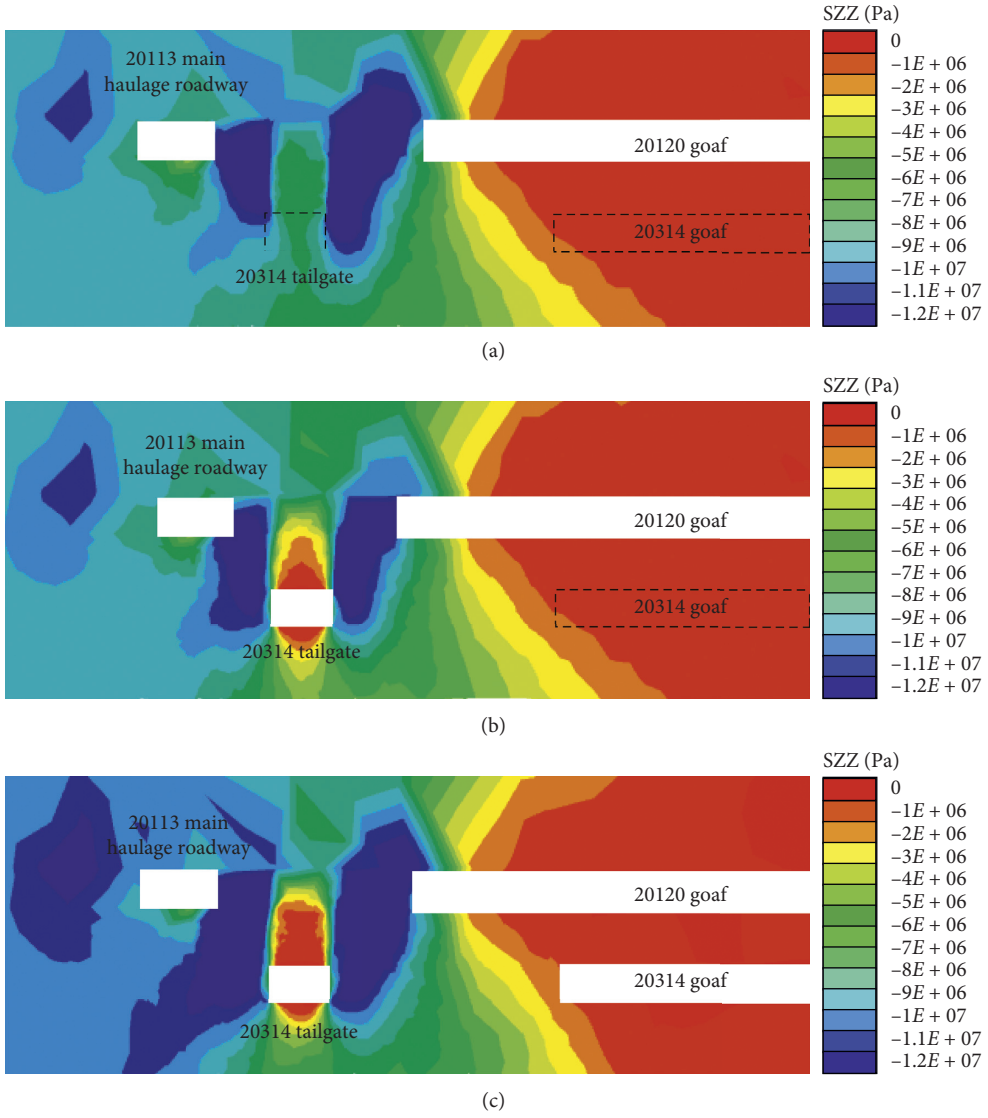

Figure 17: Nephogram of stress perpendicular to the section auxiliary haulage roadway (perpendicular to the axis section of the roadway): (a) 2-2 upper coal seam excavation; (b) 20314 tailgate excavation; (c) 20314 panel excavation.

Combined with the laboratory experiment results, the concentrated stress on the upper corner of the 20314 goaf of the roadway roof after the excavation of the P20314 working face is 11~12 MPa. The data are similar to the long-term strength of the roof strata, resulting in the creeping failure of the 20314 auxiliary transport roadway roof under the residual coal pillar, which caused the deformation and instability of the surrounding rock of the roadway.

6. Discussion

The roof bolt of the 20314 auxiliary haulage roadway eliminates the mutual dislocation between the rock strata of the roadway roof and makes the roof combine into a thicker roof structure of the composite rock beam. Meanwhile, due to the increase in thickness of the roof rock beam, the overall stability of the roof is improved and pressure on the roadway weakens. Besides, the span of the caving arch correspondingly reduces. Combined with relevant research studies, the mechanical model of the composite suspended rock beam is established, as shown in Figure 20. In the model, the stress acting on the structure of the roof rock beam is defined as q, the supporting stress of the roof anchor cable, the bolt, and the hydraulic prop is defined as q_1, and the constraining force at both ends are defined as R_O and R_B.

According to the mechanical equilibrium, the following conditions can be obtained:

$$\begin{aligned} \sum F_y &= 0, \\ \sum M_o &= 0. \end{aligned} \tag{4}$$

An equation according to the force balance and moment balance can be obtained as follows:

$$R_{oy} = R_{by} = \frac{l(q - q_1)}{2}. \tag{5}$$

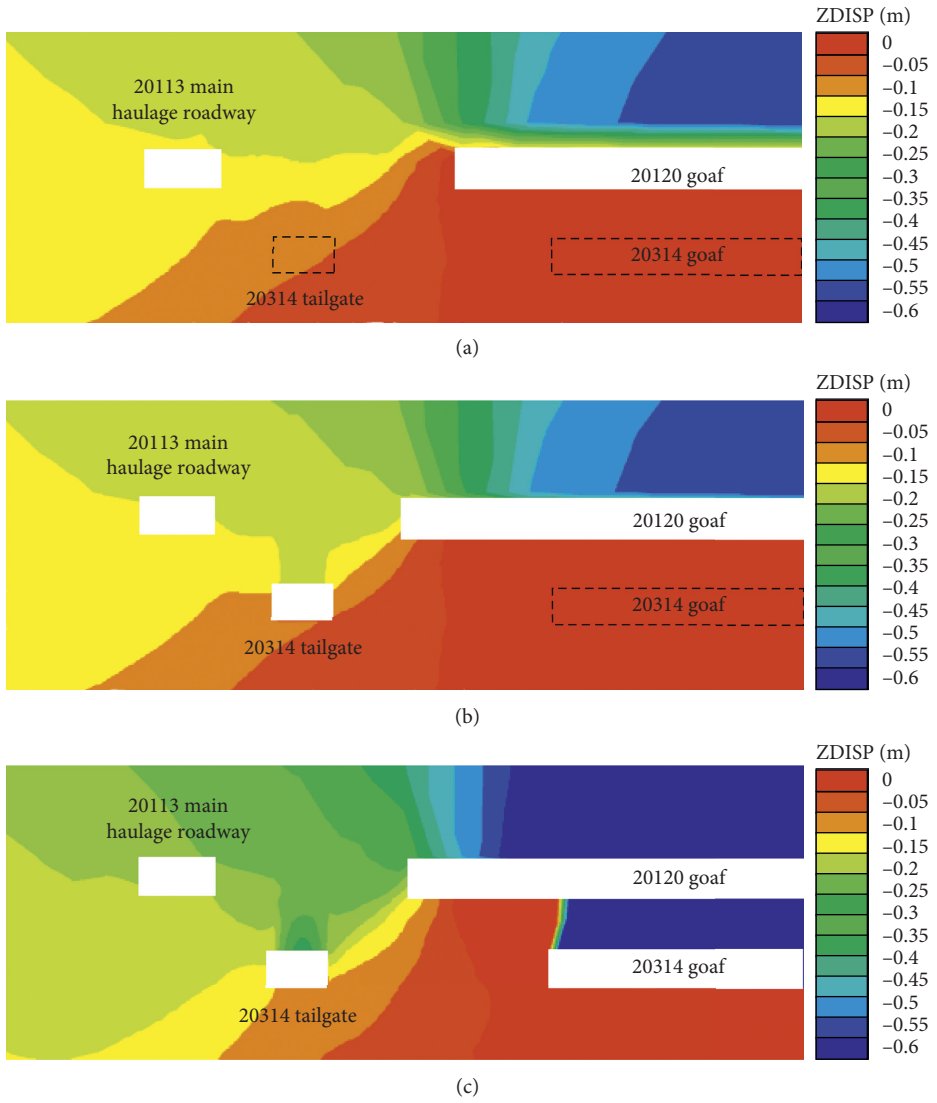

Figure 18: Displacement nephogram perpendicular to the auxiliary haulage roadway (perpendicular to the axis section of the roadway): (a) 2-2 upper coal seam excavation; (b) 20314 tailgate excavation; (c) 20314 panel excavation.

The bending moment on any section of the roof rock beam is

$$M(x) = \frac{1}{2}(q - q_1)x^2 - \frac{1}{2}(q - q_1)lx. \tag{6}$$

The maximum tensile stress of the roof rock beam is

$$\sigma_{\max} = \frac{M_{\max}}{W} = \frac{l^2(q - q_1)/8}{h_1^2/6} = \frac{3l^2(q - q_1)}{4h_1^2}. \tag{7}$$

The condition of no failure of the roof rock beam is

$$\sigma_{\max} \le [\sigma], \tag{8}$$

where l (m) represents the net width of the roadway, h_1 (m) represents the thickness of the composite suspended rock beam, and the effective length of the top bolt is taken, and q (Pa) represents the force of the overburden on the rock beam structure when the pressure is applied. According to the load estimation method, it can obtained that $q = Km\gamma$ where m (m) refers to the thicknesses sum of the interval rock (including the thickness of the upper coal seam), the immediate roof, and the main roof of the upper coal seam working face, while γ (N/m^3) represents the bulk density of overburden; K represents the dynamic load coefficient, and q_1 is the force exerted by the single hydraulic prop, bolt, and anchor cable on the roof rock beam. Furthermore, q_1 is simplified as a vertical-upward uniform load (Pa), which can be calculated as

$$q_1 = \frac{P_g}{S_b^2} + \frac{mP_s}{nlS_b} + \frac{4P_z}{(l \times 1)}, \tag{9}$$

in which P_g symbolizes the anchoring force of the bolt, P_s is the anchoring force of the cable, P_z refers to the rated working resistance of the single hydraulic props, S_b represents the spacing between the anchors, and m is the number of anchors per row. The spacing of the anchor row nS_b is an integral multiple of the row distance of the bolt in which n

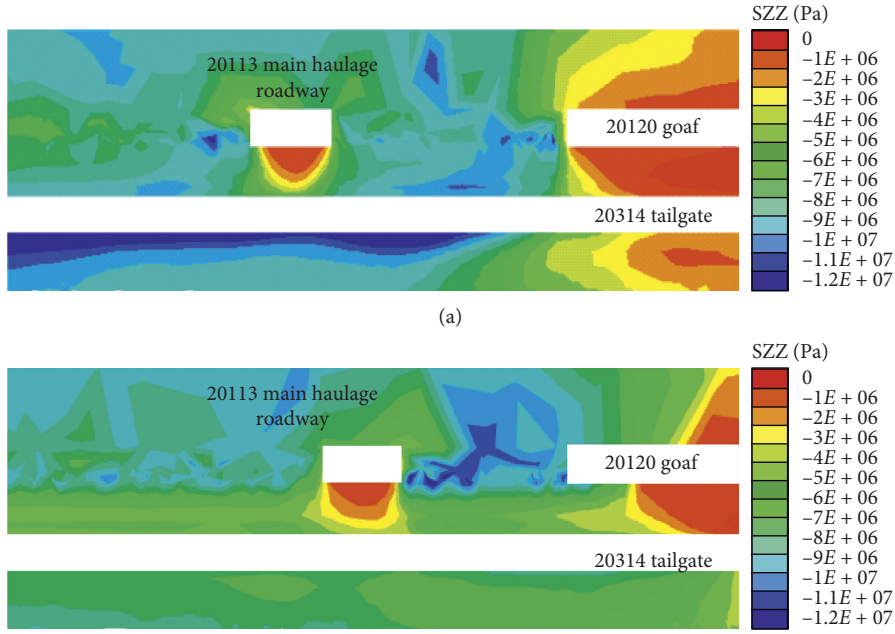

Figure 19: Stress on both sides of the roof of the 2031 auxiliary haulage roadway: (a) coal pillar side; (b) entity coal side.

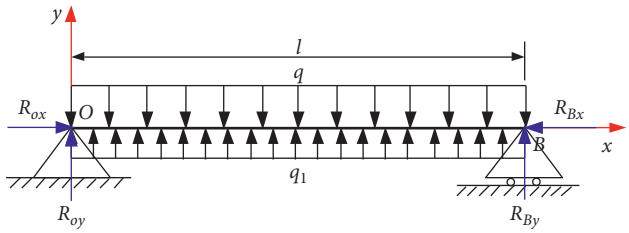

Figure 20: Mechanical model of the composite suspended rock beam structure.

takes a positive integer 1, 2, 3, . . ., σ_{max} (Pa) symbolizes the maximum tensile stress of the roof rock beam, and σ (Pa) is the tensile strength of the roof strata after anchoring.

For the auxiliary haulage roadway of the P20314 working face, the net width l is 5.2 m, the effective length h_1 of the top bolt is 2.05 m, and the spacing S_b between the anchors is 0.8 m. Figure 3 is selected for m and n. And, the maximum thickness sum (m) of the interval rock (including the upper coal seam), the immediate roof, and the main roof of the working face in the upper coal seam is 30 m. The uniform load q_1 of the anchor cable, bolt, and single hydraulic strut on the roof rock beam is 356.73 kN/m^2 (where P_g and P_s of the anchor anchoring force are 80 kN and 164 kN, respectively, and the rated working resistance of the single hydraulic prop is 250 kN).

6.1. Under Pressure of Overlying Strata Weight. Substituting the above parameters into equation (9), it can be obtained that the maximum tensile stress on the roof rock beam is 1.9 MPa. According to relevant research studies, the tensile strength of the rock after anchoring can generally reach from 5 MPa to 8 MPa around. It can be known that the maximum tensile stress on the roof rock beam is less than the tensile strength of the roof after anchoring. Consequently, the support system can play the role of controlling the surrounding rock when considering the overburden weight only.

6.2. Under Pressure of Stress Concentration. With the stopping of the P20314 working face, the 20314 auxiliary haulage roadway is located under the edge of the residual coal pillar, resulting in the superimposed bearing pressure of the two working faces (working faces of 20113 and 20120 in the 2-2 upper coal seam). Therefore, coefficient 3 is taken as the stress concentration. Substituting the relevant parameters into equation (9), it can be known that the maximum tensile stress on the roof rock beam is 9.14 MPa. Based on relevant research studies, the tensile strength of the rock after anchoring can generally reach from 5 MPa to 8 MPa around. It can be seen that the maximum tensile stress on the roof rock beam is greater than the tensile strength of the roof rock after anchoring. As a result, when considering stress concentration, the supporting system cannot effectively control the surrounding rock, and auxiliary support measures such as shed supporting must be adopted.

Therefore, the roadway of the lower coal seam should be reasonably arranged to avoid the deformation and failure of its surrounding rock during the mining of multiple and close-distance coal seams [43, 44]. The reason lies in that the roadway of the lower coal seam is different in the solid coal of the upper coal seam, the residual coal pillar, and the goaf. By a perfect arrangement, it can avoid the problem that the roadway penetrates the residual coal pillar in the upper coal seam and the phenomenon of deformation and failure

caused by the excessive stress of the surrounding rock of the roadway. If the roadway arranged must penetrate the residual coal pillar in the upper coal seam due to some reasons such as coal seam occurrence and fault, some measures can be adopted according to the specific production geological conditions of the site. Under this condition, support of the high-strength and high-pretension bolt, active support of anchor cable reinforcement, passive support of the combination of the steel beam and the single hydraulic prop, and surrounding rock grouting reinforcement can be selected [41, 45–47].

7. Conclusion

In this paper, rheological failure mechanism of the weakly cemented soft rock roadway under the residual coal pillar during the mining of shallow-buried close-distance coal seams of the Gaojialiang coal mine is analyzed and studied through field monitoring, numerical simulation, and laboratory experiment. The field monitoring results show that the data of each monitoring device in the auxiliary haulage roadway start to change at the same time, and they are stable again after changing at the same time at a slower speed. Moreover, the monitoring results of the damaged areas observed by the borehole drilling TV are consistent with the displacements of the deep roofs, which prove the reliability of the monitoring data.

The results of numerical simulation suggest that the stress of the roadway roof increases first and then decreases and increases finally. Meanwhile, after the mining of the P20314 working face, the stress and displacement of the roof of the auxiliary haulage roadway under the residual coal pillar are concentrated and increased, respectively. The results comply with the variation data of the stress and displacement of field monitoring at the 5#-1 station. Besides, the side roof stress of the P20314 working face goaf is more concentrated, which is also in line with the step-type subsidence of the side roof.

The laboratory experiment shows that the roof strata belong to the weakly cemented strata, and the specimen can creep under a small pressure. On this basis, the failure mechanism of the 20314 auxiliary haulage roadway is analyzed.

(1) Coal pillar is left because of the mining of the upper coal seam. With the excavation of the upper coal seam, the stress on the roof of the 20314 auxiliary haulage roadway under the coal pillar gradually increases and is concentrated. However, the excavation of 20314 brings in the fact that the stress on the roof is partially released and reduces further. Therefore, the surrounding rock of the roadway holds its integrity.

(2) With the stopping of the P20314 working face in the lower coal seam, the goaf of the overlap part of the upper and lower coal seams is connected, and the rotation of the overlying fractured rock makes the stress of the residual coal pillar to increase. The concentrated stress is transferred to the top of the auxiliary haulage roadway roof through the residual coal pillar, and the stress concentration area is located right above the roof. But, due to the shallow burial of the coal seam, the concentrated stress is not high enough to cause the deformation of the roadway roof directly. Instead, the roof creeps with time under such a condition, and the surrounding rock of the roadway is deformed.

(3) Through analysis, it is suggested that in the design of the working system, a gateroad under an isolated residual coal pillar in the upper coal seam should be avoided when mining in close-distance seams. If it cannot be avoided, combined supports of passive plus active measures should be used to support the roadway to ensure the safety production of coal mines.

Data Availability

The data used to support the findings of this study are included within the article.

Conflicts of Interest

The authors declare that they have no conflicts of interest regarding the publication of this paper.

Acknowledgments

The authors gratefully acknowledge that this work was supported by the National Key R&D Program of China (2018YFC0604703), Natural Science Foundation of Shandong Province (ZR2017BEE013), Research Fund of the State Key Laboratory of Coal Resources and Safe Mining, CUMT (SKLCRSM19KF016), National Natural Science Foundation of China (51574154 and 51904166), Major Program of Shandong Province Natural Science Foundation (ZR2018ZA0603), Key R&D Program of Shandong Province (2018GSF116003), and Scientific Research Foundation of Shandong University of Science and Technology for Recruited Talents (2017RCJJ009).

References

[1] Y. L. Tan, T. B. Zhao, and Y. X. Xiao, "In situ investigations of failure zone of floor strata in mining close distance coal seams," *International Journal of Rock Mechanics and Mining Sciences*, vol. 47, no. 5, pp. 865–870, 2010.

[2] J. X. Yang, C. Y. Liu, and B. Yu, "Roof structure of close distance coal strata in multi-gob condition and its effects," *Acta Geodynamica et Geomaterialia*, vol. 11, no. 4, pp. 351–359, 2014.

[3] H. Yan, M.-Y. Weng, R.-M. Feng, and W.-K. Li, "Layout and support design of a coal roadway in ultra-close multiple-seams," *Journal of Central South University*, vol. 22, no. 11, pp. 4385–4395, 2015.

[4] W.-B. Zhu, J.-L. Xu, X. Kong, D.-Y. Xuan, and W. Qin, "Study on pillar stability of wongawilli mining area in shallow close distance coal seams," *Procedia Earth and Planetary Science*, vol. 1, no. 1, pp. 235–242, 2009.

[5] Q. Bai, S. Tu, F. Wang, and C. Zhang, "Field and numerical investigations of gateroad system failure induced by hard roofs in a longwall top coal caving face," *International Journal of Coal Geology*, vol. 173, pp. 176–199, 2017.

[6] Q. Liu, W. Nie, Y. Hua, H. Peng, C. Liu, and C. Wei, "Research on tunnel ventilation systems: dust diffusion and pollution behaviour by air curtains based on CFD technology and field measurement," *Building and Environment*, vol. 147, pp. 444–460, 2019.

[7] J. Wang, J. G. Ning, L. S. Jiang, J.-Q. Jiang, and T. Bu, "Structural characteristics of strata overlying of a fully mechanized longwall face: a case study," *Journal of the Southern African Institute of Mining and Metallurgy*, vol. 118, no. 11, pp. 1195–1204, 2018.

[8] J. Wang, J. Ning, P. Qiu, S. Yang, and H. Shang, "Microseismic monitoring and its precursory parameter of hard roof collapse in longwall faces: a case study," *Geomechanics and Engineering*, vol. 17, no. 4, pp. 375–383, 2019.

[9] M. Hu, W. Zhao, Z. Lu, J. Ren, and Y. Miao, "Research on the reasonable width of the waterproof coal pillar during the mining of a shallow coal seam located close to a reservoir," *Advances in Civil Engineering*, vol. 2019, Article ID 3532784, 14 pages, 2019.

[10] H. Shang, J. Ning, S. Hu, S. Yang, and P. Qiu, "Field and numerical investigations of gateroad system failure under an irregular residual coal pillar in close-istance coal seams," *Energy Science & Engineering*, vol. 7, no. 6, pp. 2720–2740, 2019.

[11] L. Xinjie, L. Xiaomeng, and P. Weidong, "Analysis on the floor stress distribution and roadway position in the close distance coal seams," *Arabian Journal of Geosciences*, vol. 9, no. 2, p. 83, 2016.

[12] J. X. Yang, C. Y. Liu, and Y. Yang, "Study of the bearing mechanism of the coal roof and the dimension selection of the room and pillar in the shallow and close distance coal seam," *Journal of China University of Mining & Technology*, vol. 42, no. 2, pp. 161–168, 2013.

[13] Q. Gu, W. Ru, Y. Tan, J. Ning, and Q. Xu, "Mechanical analysis of weakly cemented roof of gob-side entry retaining in fully-mechanized top coal caving mining," *Geotechnical and Geological Engineering*, vol. 37, no. 4, pp. 2977–2984, 2019.

[14] X. Z. Lyu, Z. Zhao, X. Wang, and W. Wang, "Study on the permeability of weakly cemented sandstones," *Geofluids*, vol. 2019, Article ID 8310128, 14 pages, 2019.

[15] S. Zhang, G. Fan, D. Zhang, M. Chen, and C. Zhang, "Study on material properties and similar material proportion of weakly cemented water-resisting strata," *Arabian Journal of Geosciences*, vol. 12, no. 11, 2019.

[16] Q.-B. Meng, L.-J. Han, W.-G. Qiao, D.-G. Lin, and L. Yang, "Mechanism of rock deformation and failure and monitoring analysis in water-rich soft rock roadway of western China," *Journal of Coal Science and Engineering (China)*, vol. 18, no. 3, pp. 262–270, 2012, in Chinese.

[17] J. Zhu, C. Qiao, and Y. Song, "Effect of particle characteristics on shear strength of weakly cemented conglomerate in tertiary," *Journal of Harbin Institute of Technology*, vol. 5, no. 51, pp. 101–109, 2019, in Chinese.

[18] C. Y. Song, H. G. Ji, and H. Y. Jiang, "Influence of wetting-drying cycles on acoustic emission characteristics and microstruc-ture deterioration of weak cementation stratum," *Journal of China Coal Society*, vol. 43, no. 1, pp. 96–103, 2018, in Chinese.

[19] E. Maranini and M. Brignoli, "Creep behaviour of a weak rock: experimental characterization," *International Journal of Rock Mechanics and Mining Sciences*, vol. 36, no. 1, pp. 127–138, 1999.

[20] S. Liang, X. Li, Y. Mao, and C. Li, "Time-domain characteristics of overlying strata failure under condition of longwall ascending mining," *International Journal of Mining Science and Technology*, vol. 23, no. 2, pp. 207–211, 2013.

[21] S. Yin, W. Nie, Q. Liu, and Y. Hua, "Transient CFD modelling of space-time evolution of dust pollutants and air-curtain generator position during tunneling," *Journal of Cleaner Production*, vol. 239, Article ID 117924, 2019.

[22] Y. L. Li, "Experimental study of creep properties of silty mudstone under triaxial compression," *Journal of Sichuan University (Engineering Science Edition)*, vol. 44, no. 1, pp. 14–19, 2012, in Chinese.

[23] L. Kong, Y. Wang, and S. Li, "Analysis on overburden strata movement law of coal mining face under goaf of room and pillar mining face," *Coal Science & Technology*, vol. 43, no. 5, pp. 26–29, 2015, in Chinese.

[24] N.-C. Zhang, N. Zhang, J. Esterle, J.-G. Kan, Y.-M. Zhao, and F. Xue, "Optimization of gateroad layout under a remnant chain pillar in longwall undermining based on pressure bulb theory," *International Journal of Mining, Reclamation and Environment*, vol. 30, no. 2, pp. 128–144, 2016.

[25] C. Mark, F. Chase, and A. Campoli, *Analysis of Retreat Mining Pillar Stability*, West Virginia University, Morgantown, WV, USA, 1995.

[26] J. Wang, J. G. Ning, and P. Q. Qiu, "Microseismic monitoring and its precursory parameter of hard roof collapse in longwall faces: a case study," *Geomechanics and Engineering*, vol. 17, no. 4, pp. 375–383, 2019.

[27] F. H. Yu, T. B. Zhao, and Y. L. Tan, "Study on quantitative calculation method of mining roadway supporting intensity under depressurized mining," *Journal of Mining and Safety Engineering*, vol. 3, no. 33, pp. 460–466, 2016, in Chinese.

[28] R. Gao, B. Yu, and X. B. Meng, "Stress distribution and surrounding rock control of mining near to the overlying coal pillar in the working face," *International Journal of Mining Science and Technology*, vol. 29, no. 6, pp. 881–887, 2019.

[29] Z.-S. Lian, J.-R. Wang, and C.-Y. Hao, "Numerical simulation and experimental research of surrounding rock deformation of floor roadway under short-distance coal seam group combined mining," *Journal of Coal Science and Engineering (China)*, vol. 16, no. 3, pp. 230–234, 2010, in Chinese.

[30] X.-Q. Wei, H. B. Bai, H. R. Rong, Y. Jiao, and B.-Y. Zhang, "Research on mining fracture of overburden in close distance multi-seam," *Procedia Earth & Planetary Science*, vol. 2, pp. 20–27, 2011.

[31] F. He, Z. Zheng, H. Zhu, and B. Yang, "Research on failure mechanism and strengthening of broken roadway affected by upper coal pillar," *Advances in Civil Engineering*, vol. 2019, Article ID 8132817, 13 pages, 2019.

[32] J. Yang and D. Wang, "Analysis on damage characteristic of the upper coal seam mining in contiguous coal seams," *Coal Science & Technology*, vol. 7, no. 45, pp. 7–11, 2017, in Chinese.

[33] J. Zhao and G. Li, "Pressure-relief mining of the working face under the coal pillar in the close distance coal seams," *Geotechnical and Geological Engineering*, vol. 34, no. 4, pp. 1067–1077, 2016.

[34] Z. Li, H. X. Liu, Z. L. Dun, L. Ren, and J. Fang, "Grouting effect on rock fracture using shear and seepage assessment," *Construction & Building Materials*, vol. 242, 2020.

[35] T. Xiao, B. Jianbiao, X. Lei, and Z. Xuebin, "Characteristics of stress distribution in floor strata and control of roadway stability under coal pillars," *Mining Science and Technology (China)*, vol. 21, no. 2, pp. 243–247, 2011.

[36] P. Gong, T. Zhao, K. Yetilmezsoy, and K. Yi, "Mechanical modeling of roof fracture instability mechanism and its control in top-coal caving mining under thin topsoil of shallow coal seam," *Advances in Civil Engineering*, vol. 2019, Article ID 1986050, 10 pages, 2019.

[37] Y. Tan, Q. Gu, J. Ning, X. Liu, Z. Jia, and D. Huang, "Uniaxial compression behavior of cement mortar and its damage-constitutive model based on energy theory," *Materials*, vol. 12, no. 8, p. 1309, 2019.

[38] T. Li, Y. Yu, W. Cheng, Q. Xu, H. Yang, and J. Shen, "The dynamic change of pore structure for the low-rank coal with various pretreatment temperatures: a case study from southwestern ordos basin," *Geofluids*, vol. 2020, Article ID 4670812, 15 pages, 2020.

[39] W. Y. Guo, Y. Tan, F. H. Yu, and T.-B. Zhao, "Mechanical behavior of rock-coal-rock specimens with different coal thicknesses," *Geomechanics and Engineering*, vol. 15, no. 4, pp. 1017–1027, 2018.

[40] B.-Y. Jiang, S.-T. Gu, L.-G. Wang, G.-C. Zhang, and W.-S. Li, "Strainburst process of marble in tunnel-excavation-induced stress path considering intermediate principal stress," *Journal of Central South University*, vol. 26, no. 4, pp. 984–999, 2019.

[41] C. X. Wang, B. T. Shen, and J. T. Chen, "Compression characteristics of filling gangue and simulation of mining with gangue backfilling: an experimental investigation," *Geomechanics and Engineering*, vol. 20, no. 6, pp. 485–495, 2020.

[42] Z. Li, H. Zhou, D. Hu, and C. Zhang, "Yield criterion for rocklike geomaterials based on strain energy and CMP model," *International Journal of Geomechanics*, vol. 20, no. 3, 2020.

[43] M. Sun, X. Zhang, W. Zheng, and X. Zhang, "Study on causing disaster and removing danger for stress concentration of overlying residual coal pillar in ultra-close multi-seam," *Geotechnical and Geological Engineering*, vol. 37, no. 5, pp. 4009–4017, 2019.

[44] C. Xu, W. Nie, Z. Liu, H. Peng, S. Yang, and Q. Liu, "Multi-factor numerical simulation study on spray dust suppression device in coal mining process," *Energy*, vol. 182, pp. 544–558, 2019.

[45] Q. Meng, L. Han, W. Qiao, D. Lin, and J. Fan, "Support technology for mine roadways in extreme weakly cemented strata and its application," *International Journal of Mining Science and Technology*, vol. 24, no. 2, pp. 157–164, 2014.

[46] Q. Meng, L. Han, J. Sun, F. Min, W. Feng, and X. Zhao, "Experimental study on the bolt-cable combined supporting technology for the extraction roadways in weakly cemented strata," *International Journal of Mining Science and Technology*, vol. 25, no. 1, pp. 113–119, 2015.

[47] S. Hu, Y. Tan, H. Zhou et al., "Anisotropic modeling of layered rocks incorporating planes of weakness and volumetric stress," *Energy Science & Engineering*, vol. 8, no. 3, pp. 789–803, 2020.